Published in final edited form as:

Epilepsia. 2022 May ; 63(5): 1225–1237. doi:10.1111/epi.17191.

Using MR Fingerprinting to Characterize Periventricular Nodular Heterotopias in Pharmacoresistant Epilepsy

Joon Yul Choi[1], **Balu Krishnan**[1], **Siyuan Hu**[2], **David Martinez**[1], **Yinging Tang**[1,3], **Xiaofeng Wang**[4], **Ken Sakaie**[5], **Stephen Jones**[5], **Hiroatsu Murakami**[1], **Ingmar Blümcke**[1,6], **Imad Najm**[1], **Dan Ma**[2,†], **Zhong Irene Wang**[1,†]

[1]Epilepsy Center, Neurological Institute, Cleveland Clinic, Cleveland, OH 44195, USA

[2]Biomedical Engineering, Case Western Reserve University, Cleveland, OH 44106, USA

[3]Department of Neurology, West China Hospital of Sichuan University, Chengdu, Sichuan 610041, China

[4]Quantitative Health Science, Cleveland Clinic, Cleveland, OH 44195, USA

[5]Imaging Institute, Cleveland Clinic, Cleveland, OH 44195, USA

[6]Neuropathology, University of Erlangen, Erlangen 91054, Germany

Summary

Objective: We aimed to use a novel magnetic resonance fingerprinting (MRF) technique to examine *in vivo* tissue property characteristics of periventricular nodular heterotopias (PVNHs). These characteristics were further correlated with stereotactic-EEG (SEEG) ictal onset findings.

Methods: We included 5 patients with PVNH who had SEEG-guided surgery and at least one-year seizure freedom or substantial seizure reduction. High-resolution MRF scans were acquired at 3T, generating 3D quantitative T_1 and T_2 maps. We assessed the differences between T_1 and T_2 values from the voxels in the nodules located in the SEEG-defined SOZ and non-SOZ, on individual-level and group-level. ROC analyses were performed to obtain the optimal classification performance. Quantification of SEEG ictal onset signals from the nodules was performed by calculating power spectrum density (PSD). The association between PSD and T_1/T_2 values were further assessed at different frequency bands.

Results: Individual-level analysis showed T_1 was significantly higher in SOZ voxels than non-SOZ voxels ($p < 0.05$), with an average 73% classification accuracy. Group-level analysis also

[†]Co-correspondence: Dan Ma, PhD, Department of Biomedical Engineering, Case Western Reserve University, B110 Bolwell Building, 11100 Euclid Avenue, Cleveland, OH, 44106, USA, dan.ma@case.edu, Zhong Irene Wang, PhD, Epilepsy Center, Cleveland Clinic, Desk S-51, 9500 Euclid Avenue, Cleveland OH 44195, USA, wangi2@ccf.org.

Conflict of interest

Imad Najm is on the Speakers' bureau of Eisai. Stephen Jones received travel and speaker fees from SIEMENS Healthineers. Other authors have no competing interests to disclose.

Ethical Publication Statement

We confirm that we have read the journal's position on issues involved in ethical publication and affirm that this report is consistent with those guidelines.

Supporting information

Supplementary material is available at *Epilepsia* online.

showed higher T_1 was significantly associated with SOZ voxels ($p < 0.001$). At the optimal cut-off (normalized T_1 of 1.1), a 76% accuracy for classifying SOZ nodules from non-SOZ nodules was achieved. T_1 values were significantly associated with ictal-onset PSD at the ultra-slow, θ, β, γ, and ripple bands ($p < 0.05$). T_2 values were significantly associated with PSD only at the ultra-slow band ($p < 0.05$).

Significance: Quantitative MRF measures, especially T_1, can provide additional noninvasive information to separate nodules in SOZ and non-SOZ. The T_1 and T_2 tissue property changes carry electrophysiological underpinnings relevant to the epilepsy, as shown by their significant correlations with power changes during the SEEG seizure onset. The use of MRF as a fementary noninvasive tool may improve presurgical evaluation for patients with PVNH and pharmacoresistant epilepsy.

Keywords

Periventricular nodular heterotopia; Magnetic resonance imaging; MR fingerprinting; Stereotactic-electroencephalography (SEEG); T1 relaxation time

Introduction

Periventricular nodular heterotopias (PVNHs, or nodules) are brain malformations due to abnormal neuronal migration during cortical development[1–4] and are frequently associated with pharmacoresistant epilepsy.[5,6] Surgical resection or ablation of the epileptogenic zone is the most effective intervention to achieve seizure freedom in patients with pharmacoresistant epilepsy. However, localizing the epileptogenic zone in epilepsies associated with PVNH is challenging. There is a lack of clear structural or metabolic biomarkers of *in vivo* epileptogenicity for the nodules. In addition, complex and heterogeneous interactions between the nodules and their overlying neocortex often present.[7] Although invasive evaluation with stereotactic-electroencephalography (SEEG) is a necessary step for the localization of epileptogenic zones in patients with PVNH, SEEG electrodes cannot fully sample the many and frequently bilateral nodules for practical reasons. This challenge often results in incomplete information about the epileptogenic nature of some of the nodules even after an extensive SEEG evaluation.

MRI is a powerful imaging tool to detect epileptic lesions non-invasively. On conventional T_1 weighted (T_{1w}) and T_2 weighted (T_{2w}) images, PVNH lesions tend to have uniform signal intensity and cannot distinguish epileptic nodules from the non-epileptic ones. Thus, there is a need for an MRI method that is both more sensitive to brain tissue property changes and specific to the epileptic potential of PVNH.

Magnetic resonance fingerprinting (MRF) is a novel MRI technique that utilizes variable acquisition patterns (e.g. variable flip angles and repetition times) to generate perfectly-aligned, high-resolution quantitative tissue property maps (T_1 and T_2 maps) in clinically feasible time.[8,9] The quantitative MRF T_1 and T_2 tissue property maps have shown improved sensitivity, specificity, and repeatability in various clinical applications.[10–12] As demonstrated in prior studies, T_1 and T_2 values may carry diagnostic significance for epileptic lesions such as hippocampal sclerosis[12] and cortical malformations.[9] In particular,

our prior study used the 3D MRF method to investigate a cohort of pharmacoresistant epilepsy patients with focal cortical dysplasia (FCD), PVNH and tuberous sclerosis complex. We demonstrated initial efficacy of the MRF T_1 and T_2 tissue property maps, showing differentiating signals when multiple lesions were present, while conventional MRI was uninformative.[9] This motivated the current study to systematically examine the efficacy of 3D MRF to probe the *in vivo* epileptogenicity of PVNH lesions.

In this study, we aim to investigate differences between quantitative T_1 and T_2 values in nodules from the SOZ and non-SOZ, at the individual-level and group-level. We further explored the electrophysiological underpinnings of quantitative T_1 and T_2 values, and assessed their relationship with power spectral density (PSD) at SEEG ictal onset. We hypothesize that T_1 and T_2 values from MRF could carry quantitative tissue property information to differentiate nodules in the SOZ from those in the non-SOZ, and they would have significant positive correlations with power changes during the SEEG seizure onset, as quantified by PSD.

Materials and methods

Patient selection

From a consecutive cohort of pharmacoresistant epilepsy patients undergoing presurgical evaluation at the Cleveland Clinic Epilepsy Center from 2017 to 2020, patients were retrospectively included based on the following selection criteria: (1) had PVNH lesions on the 3T clinical MRI with no other malformations in the cortex, based on official radiology report; (2) underwent a 3D whole-brain MRF scan; (3) underwent SEEG as part of their presurgical evaluation, with at least one electrode targeting the nodules; (4) underwent resective or ablative surgery; (5) had at least one-year seizure freedom or substantial seizure reduction after surgery. Exclusion criteria: severe imaging artifacts preventing image segmentation or registration. Analyses of this study was performed retrospectively, and none of the results influenced clinical recommendation. This study was approved by the Institutional Review Board (IRB) of the Cleveland Clinic and all subjects gave written informed consent to participate in the MRF research scan.

MRI acquisition

A 3D whole-brain MRF scan was acquired on a 3T MRI (Prisma, Siemens, Erlangen, Germany) with field of view (FOV) = 300 × 300 × 144 mm^3, resolution = 1 × 1 × 1 mm^3 and scan time = 10 min 40 sec.[8,9] In addition to the MRF scan, a 3D B_1 mapping scan was acquired with the same FOV and resolution as the MRF scan to compensate for the B_1 inhomogeneity in MRF maps (scan time = 1 min 50 sec).[13–15] To estimate T_1 and T_2 values of each voxel, the acquired MRF signals were matched to a predefined signal evolution dictionary that was generated by Bloch equation simulation (T_1 range: 2 – 3000 ms and T_2 range: 3 – 2000 ms) using a pattern recognition method.[9] Representative MRF T_1 and T_2 maps are shown in Figure 1. A clinical 3D T_{1w} whole-brain magnetization-prepared rapid acquisition with gradient echo (MPRAGE) scan was additionally acquired with the following parameters: resolution = 0.5 × 0.5 × 0.9 mm^3, repetition time (TR) = 1900 ms,

echo time (TE) = 2.57 ms, inversion time (TI) = 1100 ms, 192 slices and scan time = 3 min 53 sec.

Data processing

SEEG electrode reconstruction was performed by fusing the postoperative thin-sliced CT images with the preoperative clinical T_{1w} MPRAGE images using automatic full-volume maximal-mutual-information registration in Curry 8 (Compumedics NeuroScan, Australia). Classification of SOZ and non-SOZ SEEG contacts were obtained from the official clinical report, based on consensus at the epilepsy patient management conference (PMC).

MRF T_{1w} images were synthesized from the MRF maps, with a contrast similar to the T_{1w} MPRAGE images obtained from conventional clinical protocol. MRF T1w images were registered to T1w MPRAGE images using symmetric image normalization (SyN) in advanced normalization tools (ANTs).[16] SyN was used as it was shown to consistently deliver high accuracy of registration results.[17] The warping information from the registration of MRF T_{1w} images was applied to T_1 and T_2 maps, to register them to the T_{1w} MPRAGE images. Overall, this process allowed for the T_{1w} MPRAGE images, T_1 map, T_2 map, and SEEG electrode location to be registered in the same space.

Segmentation of PVNH lesions

A diagram for PVNH lesion mask generation is shown in Figure 2(A). The T_{1w} MPRAGE image was segmented to obtain a cerebral spinal fluid (CSF) mask using FSL (FMRIB, Oxford, UK).[18] Then, a whole-brain mask of T_1 and T_2 maps was subtracted by the CSF mask, and neighboring voxels closed to CSF were excluded in the subtracted mask to avoid partial volume effects from CSF. To precisely remove voxels of white matter within the PVNH lesion mask, a histogram of T_1 values of the whole brain was fit to a three exponential Gaussian curve to calculate an average and standard deviation of white matter values,[19] as shown in Figure S1. The average white matter value plus three standard deviations of white matter was used as a threshold to remove the white matter voxels in the subtracted mask for each patient. Lastly, the centroid of each nodule was defined by expert review of the lesion mask, and an ROI with a radius of 3 mm was applied at the centroid to generate the individual nodule lesion mask. The radius of 3mm was chosen empirically to ensure full coverage of all the nodules with no overlap. If the nodule was sampled with SEEG, the centroid of the ROI was set at the contact. We then multiplied the ROIs with the nodule lesion masks to extract MRF T_1 and T_2 values within each ROI.

Definition of SOZ and non-SOZ nodules

If the nodules were implanted by SEEG and included in the SOZ (per official clinical report), they were considered SOZ nodules. If nodules were implanted by SEEG and shown to be not involved at SOZ, they were considered non-SOZ nodules. If the nodules were not implanted by SEEG (per PMC consensus based on noninvasive evaluation data), they were also considered as non-SOZ nodules; this was a fair assumption given the patients included in this cohort had sustained seizure freedom or significant seizure reduction after the SEEG-directed surgery which did not involve these nodules. Whenever possible, post-operative MR images were coregistered to confirm non-SOZ nodules were outside of surgical cavity.

Data analysis

Analysis of MRF T_1 and T_2 values—All statistical analyses were performed using MATLAB 2020a (Mathworks, Natick, MA). For individual-level analysis, a t-test was performed to investigate the statistical difference between T_1 and T_2 values from the voxels in the nodules located in the SOZ and non-SOZ. T_1 and T_2 values of SOZ and non-SOZ voxels were used to create receiver operating characteristic (ROC) curves. Youden index was used to identify the optimal cut-off value of T_1 and T_2 for SOZ and non-SOZ voxels. The classification performance metrics included accuracy (ACC), sensitivity (SEN), specificity (SPE) and area under the ROC curve (AUC).

For group-level analysis, linear mixed-effects models (LMMs) were fitted to investigate the association between T_1 and T_2 values and SOZ/non-SOZ voxels: T_1 or T_2 = response variable, SOZ/non-SOZ = predictor variable (fixed effects) and patient = random effects.

Furthermore, for group-level analysis, we proposed a normalized cut-off of T_1 value between SOZ and non-SOZ nodules using datasets from all patients based on Youden index, as shown in Figure S2. Mean T_1 values for each nodule were used to generate a group-level ROC curve. The mean T_1 value of the whole-brain gray matter was used to normalize T_1 values of nodules in each patient to minimize individual heterogeneities.

Analysis of relationship between SEEG power spectral density and MRF values—Quantification of SEEG ictal onset characteristics was performed by estimating the PSD from signals at the ictal onset on the SEEG contacts located in the SOZ and non-SOZ nodules, as shown in Figure 2(B). One patient (P4) was excluded from this part of the analysis because there were no electrode contacts placed in non-SOZ nodules, preventing comparisons. SEEG data (sampling frequency = 1000 Hz) was analyzed using a referential montage and a single electrode placed on the scalp was used as reference. PSD analyses were performed using Morlet wavelet decomposition. The average spectral power in the following frequency bands was estimated: ultra-slow (< 0.5Hz), δ (0.5 – 4Hz), θ (4 – 8Hz), α (8 – 12Hz), β (12 – 30Hz), γ (30 – 100Hz), and ripple (100 – 200Hz). We performed analyses using 5-second, 10-second and 20-second windows following the SEEG seizure onset, using the same onset markings as the ones used for clinical purpose. Median duration of all the seizures included in the PSD analyses was 97 sec (range: 22 to 163 sec). Ictal onset patterns were typically characterized by pre-ictal spiking (or burst of polyspikes) followed by a sudden burst of tonic fast activities, observed over slow waves evolving to a progressively building up pattern. To quantify the relative change in power, the average spectral power from a 5-minute segment of baseline SEEG data was estimated. Normalized spectral power at seizure onset was estimated for each SEEG contact by subtracting the mean spectral power from the baseline and dividing it by the standard deviation of spectral power from the baseline. We used average normalized PSD across multiple seizures for each patient to minimize bias.

To explore the relationship between normalized PSD and mean T_1 or T_2 values for the nodules, LMMs were fitted to datasets of all patients: PSD = response variable, T_1 or T_2 = predictor variable (fixed effects) and patient = random effects.

Results

From 2017 to 2020, a total of 20 patients with PVNH underwent presurgical evaluation, and 15 patients had MRF acquired. Twelve of the 15 patients underwent SEEG and then resective/ablative surgery, and 7 patients had one-year post-op follow up. Eventually, 5 patients fulfilled the inclusion criteria. At one-year post-op follow up, 3 patients were completely seizure-free and aura-free (ILAE Class 1); one patient was seizure-free but had occasional auras (ILAE Class 2); and one patient had only two seizures after surgery as compared to weekly seizures before (ILAE Class 3). Detailed demographics and clinical information can be found in Table 1. Figure 1 shows MRF T_1 and T_2 maps, as well as the locations of coregistered SEEG electrodes. Visual inspection of the clinical MRI could not differentiate any signal differences amongst the nodules in any of the included patients. All SOZ nodules were sampled and confirmed by SEEG; 59% of the non-SOZ nodules were sampled and confirmed by SEEG, while 41% of the non-SOZ nodules were not implanted.

MRF individual-level analyses

Figure 3 shows violin plots of MRF T_1 and T_2 values of voxels from SOZ and non-SOZ nodules for each patient. As shown in Figure 3A and Table 2, the mean T_1 values were significantly higher in the SOZ voxels than the non-SOZ voxels for all patients ($p < 0.05$, average 14% higher in SOZ). Mean MRF T_2 value changes were not consistent across patients (Figure 3B and Table 2): patients 1 and 5 had increased T_2 in SOZ voxels; patients 2 and 3 had decreased T_2 in SOZ voxels; patient 4 showed no significant changes. This finding was consistent when comparing the SOZ and the SEEG-sampled non-SOZ nodules ($p < 0.001$).

Table 3 shows classification performances to differentiate voxels from SOZ and non-SOZ nodules at the individual patient-level. MRF T_1 value showed average of ACC, SEN, SPE, and AUC of 73.4%, 79.4%, 72.8%, and 0.80, respectively. The individual cut-off values of MRF T_1 with the optimal classification performance were quite variable across patients, at 1429, 1386, 1561, 1455, and 1584 ms highlighting individual heterogeneity. MRF T_2 showed less optimal performance than MRF T_1, with an average of ACC, SEN, SPE, and AUC of 61.5%, 61.2%, 67.5%, and 0.67, respectively.

MRF group-level analyses

MRF T_1 values were significantly associated with SOZ and non-SOZ voxels in LMM ($p < 0.001$). The estimated coefficient and standard error of LMM for SOZ/non-SOZ were 192.5 and 47.2, respectively. Consistent with the results from patient-level analyses, MRF T_2 was not significantly associated with SOZ and non-SOZ. Detailed fitting results are summarized in Table S1.

Since T_1 values were significantly associated with SOZ and non-SOZ at the group level, they were used to calculate a cut-off at the group level, to determine the threshold for separating SOZ and non-SOZ nodules. MRF T_1 values reveal ACC of 76.3% for the classification between SOZ and non-SOZ nodules at the group level, at the normalized

cut-off of 1.1. The optimal SEN, SPE, and AUC of T_1 were 76.9%, 76.2%, and 0.82, respectively. Figure S2-A–B shows detailed ROC analysis results.

MRF and PSD correlations

On all SEEG sampled nodules, MRF T_1 values were significantly associated with normalized PSD at the seizure onset, in the ultra-slow, θ, β, γ and ripple bands ($p < 0.05$); these significant correlations were consistently seen with 5, 10 or 20 second windows. For MRF T_2 values, significant associations were found only in the ultra-slow band ($p < 0.05$) consistently across the 5, 10 or 20 second windows.

Discussion

We present here the first study to systematically examine the efficacy of 3D MRF to probe the *in vivo* epileptogenicity of PVNH. We show that the quantitative T_1 tissue property value from MRF was significantly elevated in the epileptic (SOZ) nodules compared to non-epileptic nodules, on both individual-level and group-level analyses. This is further corroborated by the significant correlation between the quantitative T_1 and T_2 values and select frequency bands in the power spectrum density analyses based on the SEEG ictal onset data. Altogether, our findings show the potential value of the MRF quantitative tissue property maps in non-invasive localization of the epileptic nodules. One important caveat should be considered when interpreting our findings: our cohort consisted of patients with PVNH and no overt cortical malformations. PVNH can also exist with extensive cortical malformations, with even more complex and diffuse epileptic networks.[7] While clearly understanding the intricate interactions between nodules and their overlying cortex on the electrophysiological level[7], our study, as the first MRF study on patients with PVNH, focused on the imaging characteristics of the nodules themselves, not the overlying cortex. It is our hope that the current study would provide a framework for future studies using the MRF method to also investigate the complex overlying cortex in epilepsy patients with PVNH.

Contribution to the literature

PVNH is highly associated with pharmacoresistant epilepsy, and surgical management of this pathological entity is tremendously challenging. There is a high level of heterogeneity in the patients with PVNH, as the nodules can be single, multiple with unilateral distribution, multiple with bilateral distribution, and with or without complex cortical malformations. The epileptogenic role of the nodules is supported by prior studies that showed poor seizure outcomes when surgeries left nodules unresected.[4,20,21] In the meantime, there are clear indications of interactions between nodules and the overlying cortex, constituting highly individualized epileptogenic network that renders SEEG explorations indispensable.[7,22] Due to these challenges, patients with PVNH were frequently not considered favorable surgical candidates. In the literature, most previous studies with surgical outcomes are case reports or small series[4,20,21,23–27] with the largest cohort reporting on 20 patients.[7] These prior studies have a few consistent findings. First, there is an intrinsic capability for the nodules to generate seizures, therefore they constitute an important part of the epileptogenic network. Second, within the same patient, all nodules are not the same in

terms of their metabolic and electrical characteristics. Differences in fluorodeoxyglucose (FDG) uptake on PET, for example, were observed among various nodules in the same patient.[7] Interictal activities were often asynchronous among different nodules of the same patient, and seizures can start in one or a subgroup of nodules. Last, upon identification of the seizure onset zone, surgical interventions (radiofrequency thermocoagulation, laser ablation, and resective surgery) can be quite effective in achieving seizure freedom. SEEG-guided radiofrequency-thermocoagulation was reported to lead to a substantial percentage of patients with seizure freedom,[7] including patients with bilateral nodules which were traditionally considered as contraindication for surgery success. Taken together, investigation of the highly individualized epilepsies associated with PVNH, while challenging, could be fruitful for an optimal surgical plan leading to sustained seizure freedom or reduction.

Few MRI studies have been conducted to investigate PVNH. Conventional structural MRI typically exhibits isointense signal/contrast from the nodules, and therefore is not as helpful in generating focal surgical strategies, as compared to other epileptic pathologies, such as hippocampal sclerosis and FCD. Nolan et al. investigated diffusion tensor imaging and resting-state functional MRI in a single case, reporting structural and functional connections between the particular nodule and overlying cortex that was suspected to cause the seizures.[27] Differences in functional connectivity strength have also been reported between patients with PVNH and healthy controls on a group-level using resting-state functional MRI.[23,24] Deleo et al. utilized group-level quantitative image analysis to illustrate widespread structural and functional alterations in PVNH, particularly interacting with the overlying cortex and the hippocampus.[28] Our current study is the first to use a novel quantitative MRI technique (3D high-resolution MRF) to show the tissue property differences between SOZ and non-SOZ nodules as confirmed by SEEG, on both individual and group levels, therefore providing a significant addition to the literature.

Advantages of quantitative MRI

In conventional MR imaging, tissue contrast from T_{1w} and T_{2w} images originate from differences in the relaxation time (i.e. quantitative T_1 and T_2 values) of different tissue types. Although the T_{1w} and T_{2w} images often provide good tissue contrast, the signal depends on many factors such as pulse sequence types, acquisition sequence parameters, receive coil sensitivity and geometry, and hardware conditions.[29] Additionally, the signal source is a mixture of proton density and relaxation time of tissues. This non-linear blend of signal sources has limited investigation of specific tissue properties for neurological diseases. On the other hand, the 3D MRF technique we applied in the current study allows for direct, high-resolution measurement of two independent tissue property parameters, namely the quantitative T_1 and T_2 values. These values provide a direct link between the acquired signal change and the microstructural change[9–11,30], allowing for characterization of the nodules.

MRF T_1 map findings

Our data suggest that MRF T_1 tissue property maps reveal significant changes in the nodules located in the SOZ at the individual-level and group-level. T_1 relaxation time is a spin-lattice relaxation time that involves an exchange of energy between water protons and the surrounding lipid, protein, and macromolecules. On individual-level data, we showed

that MRF T_1 values in SOZ voxels were significantly higher than those in non-SOZ voxels, and revealed a high accuracy of 73% for classifying voxels resided in SOZ and non-SOZ nodules. On group-level data, T_1 was also significantly associated with SOZ or non-SOZ, and showed a high 76% accuracy to classify SOZ from non-SOZ nodules using a normalized T_1 threshold. These results carry practical significance in the clinical setting, as the high classification accuracy of the MRF T_1 tissue property map suggests that this non-invasive tool could provide additional information for the surgical planning of PVNH cases. The T_1 value *increase* found in the SOZ nodules is consistent with the trend of T_1 change found in other types of epilepsy. In a previous study, 24 patients with temporal lobe epilepsy presented with an ipsilateral distribution of T_1 increase in temporopolar, parahippocampal, and orbitofrontal cortices compared to healthy controls.[31] In another study, 33 patients with temporal lobe epilepsy showed an increase in T_1 values in both atrophic and normal-appearing hippocampus, as compared to the T_1 values from hippocampi of healthy participants.[12] Nöth et al. showed increased T_1 values in FCD lesions in 8 epilepsy patients.[32] Overall, the T1 tissue property value seems to be consistently increased in epileptogenic tissues, and our study examining PVNH also corroborates this trend.

The individual heterogeneity of the optimal T_1 cut-off values is worth noting. This variability could be physiologically related, as reported by prior studies showing age related changes of T_1 and T_2 values in the normal brain.[10,33] It could also be explained by diseased related factors such as seizure frequency, epilepsy duration and anti-seizure medications. This individual heterogeneity prompted us to adopt a normalized cut-off value, using the mean intensity of whole-brain gray matter for the normalization. Future investigations are needed to further mitigate this heterogeneity by other normalization methods. Once validated in a larger cohort, a supra-threshold nodule map (as sketched out in Figure S2-C) can be a useful non-invasive tool for SEEG planning of patients with PVNH.

MRF T_2 map findings

T_2 relaxation time is spin-spin relaxation that originates from the de-phasing of water protons due to interaction between them. On individual-level data, MRF T_2 value changes were not consistent across patients. On group-level data, T_2 was not significantly associated with SOZ or non-SOZ. The difference in the performance of T_1 and T_2 to characterize SOZ in PVNH may be explained by their distinct biophysical mechanisms. It could also be related to the relatively larger variation of T_2 measured by MRF,[34,35] partly due to B_1 inhomogeneity and large magnetization transfer effects.[36] As previous studies have reported increased T_2 values in FCD[37,38] and hippocampal sclerosis lesions,[39] future technical development is warranted for MRF T_2 map to elevate the combined efficacy of the MRF multiparametric tissue property maps.

Correlation between SEEG spectral analysis and MRF findings

The qualitative nature of conventional weighted structural MR imaging precludes direct comparisons between electrophysiology and tissue property values. Indirect associations between volumetric MRI abnormalities and electrophysiological changes have been previously reported. A prior study on temporal lobe epilepsy reported the degree of entorhinal cortex atrophy was significantly correlated with the strength of coupling between

the hippocampus and the entorhinal cortex at SEEG seizure onset.[40] Another study reported correlation between the degree of atrophy in the amygdala/hippocampal structures and SEEG background activities.[41] Different from these prior studies, our approach provides the first attempt to directly compare quantitative T_1 and T_2 values with electrophysiological changes. Focusing on PVNH lesions, we showed higher T_1 values at the nodules were significantly associated with increased power change during the seizure onset in the ultra-slow, θ, β, γ and ripple bands. T_2 showed similar significant associations, but limited to the ultra-slow band. It is intriguing to speculate what these correlations imply. Prior SEEG studies reported low-voltage fast activity was mainly seen as the ictal pattern from the nodules, typically with simultaneous involvement of the overlying cortex and sometimes alone,[7,20] suggesting the importance of the higher frequency bands in the PVNH-related epileptic network. Previous reports have also described the presence of fast activity (beyond 25 Hz) on intracranial EEG during seizure onset as a characteristic biomarker of the epileptogenic cortex.[42–44] Additionally, the presence of ultra-slow frequency activities during interictal and ictal onset within the epileptic network has also been described in humans[45–47] and computational models of epilepsies.[48] Taken together, the significant correlation between the MRF tissue property values and ictal-onset PSD could imply that these tissue property values may have strong electrophysiological underpinnings relevant to the epilepsy.

Limitations

Our study is inevitably affected by the small sample size and selection bias, with a highly selected cohort of PVNH and no overt cortical malformations. To strengthen the results, a larger sample size is very much needed. We are in the process of planning a multicenter study with a larger cohort to validate our findings in the near future. Additionally, because the image processing schemes differ significantly for PVNH and cortical regions, the current study focused on the nodules, while understanding the SOZ of patients with PVNH should also include the overlying cortex, which will be the topic of our follow up study. Of note, our framework of validating quantitative MRI findings with quantitative intracranial EEG findings can be generalized to the study of other pathologies. Lastly, the current study only included patients who became seizure-free, as it was necessary to confirm which nodules were truly epileptic and which were not. Future studies with a larger cohort should include both seizure-free and non-seizure-free patients, to assess the specificity of our findings.

Conclusion

Quantitative MRF measure, especially T_1, can provide additional noninvasive information to separate nodules in SOZ and non-SOZ on both individual-level and group-level. The T_1 and T_2 tissue property values carry electrophysiological underpinnings relevant to the epilepsy, as shown by their significant correlations with power changes during the SEEG seizure onset. Our study suggests the potential of using MRF as a supplementary noninvasive tool to improve presurgical evaluation for patients with PVNH and pharmacoresistant epilepsy.

Supplementary Material

Refer to Web version on PubMed Central for supplementary material.

Acknowledgments

This study was supported by the National Institutes of Health (NIH) [grant numbers R01 NS109439, R21 EB026764].

References

1. Barkovich AJ, Kjos OB. Gray matter heterotopias: MR characteristics and correlation with developmental and neurologic manifestations. Radiology. 1992; 182(2):493–9. [PubMed: 1732969]
2. Raymond AA, Fish DR, Stevens JM, Sisodiya SM, Alsanjari N, Shorvon SD. Subependymal heterotopia: a distinct neuronal migration disorder associated with epilepsy. J Neurol Neurosurg Psychiatry. 1994/10/01. 1994; 57(10):1195–202. [PubMed: 7931380]
3. Kuzniecky RI, Barkovich AJ. Malformations of cortical development and epilepsy. Brain Dev. 2001; 23(1):2–11. [PubMed: 11226722]
4. Li LM, Dubeau F, Andermann F, Fish DR, Watson C, Cascino GD, et al. Periventricular nodular heterotopia and intractable temporal lobe epilepsy: Poor outcome after temporal lobe resection. Ann Neurol. 1997; 41(5):662–8. [PubMed: 9153529]
5. Dubeau F, Tampieri D, Lee N, Andermann E, Carpenter S, Leblanc R, et al. Periventricular and subcortical nodular heterotopia. A study of 33 patients. Brain. 1995; 118 (Pt 5):1273–87. [PubMed: 7496786]
6. Battaglia G, Chiapparini L, Franceschetti S, Freri E, Tassi L, Bassanini S, et al. Periventricular Nodular Heterotopia : Classification , Epileptic History , and Genesis of Epileptic Discharges. Epilepsia. 2006; 47(1):86–97. [PubMed: 16417536]
7. Mirandola L, Mai RF, Francione S, Pelliccia V, Gozzo F, Sartori I, et al. Stereo-EEG: Diagnostic and therapeutic tool for periventricular nodular heterotopia epilepsies. Epilepsia. 2017; 58(11):1962–71. [PubMed: 28880999]
8. Ma D, Gulani V, Seiberlich N, Liu K, Sunshine JL, Duerk JL, et al. Magnetic resonance fingerprinting. Nature. 2013/03/15. 2013; 495(7440):187–92. [PubMed: 23486058]
9. Ma D, Jones SE, Deshmane A, Sakaie K, Pierre EY, Larvie M, et al. Development of high-resolution 3D MR fingerprinting for detection and characterization of epileptic lesions. J Magn Reson Imaging. 2019; 49(5):1333–46. [PubMed: 30582254]
10. Badve C, Yu A, Rogers M, Ma D, Liu Y, Schluchter M, et al. Simultaneous T1 and T2 Brain Relaxometry in Asymptomatic Volunteers Using Magnetic Resonance Fingerprinting. Tomography. 2015; 1(2):136–44. [PubMed: 26824078]
11. Badve C, Yu A, Dastmalchian S, Rogers M, Ma D, Jiang Y, et al. MR fingerprinting of adult brain tumors: Initial experience. Am J Neuroradiol. 2017; 38(3):492–9. [PubMed: 28034994]
12. Liao C, Wang BSK, Cao X, Li BSY, Wu MSD. Detection of Lesions in Mesial Temporal Lobe Epilepsy by Using MR Fingerprinting. 2018; (3):1–9.
13. Ma D, Coppo S, Chen Y, McGivney DF, Jiang Y, Pahwa S, et al. Slice profile and B1 corrections in 2D magnetic resonance fingerprinting. Magn Reson Med. 2017; 78(5):1781–9. [PubMed: 28074530]
14. Chen Y, Jiang Y, Pahwa S, Ma D, Lu L, Twieg MD, et al. MR fingerprinting for rapid quantitative abdominal imaging. Radiology. 2016; 279(1):278–86. [PubMed: 26794935]
15. Ma D, Jiang Y, Chen Y, McGivney D, Mehta B, Gulani V, et al. Fast 3D magnetic resonance fingerprinting for a whole-brain coverage. Magn Reson Med. 2018; 79(4):2190–7. [PubMed: 28833436]
16. Avants B, Gee JC. Geodesic estimation for large deformation anatomical shape averaging and interpolation. Neuroimage. 2004; 23(SUPPL. 1):S139–150. [PubMed: 15501083]
17. Klein A, Andersson J, Ardekani BA, Ashburner J, Avants B, Chiang MC, et al. Evaluation of 14 nonlinear deformation algorithms applied to human brain MRI registration. Neuroimage. 2009; 46(3):786–802. [PubMed: 19195496]
18. Zhang Y, Brady M, Smith S. Segmentation of brain MR images through a hidden Markov random field model and the expectation-maximization algorithm. IEEE Trans Med Imaging. 2001; 20(1):45–57. [PubMed: 11293691]

19. Shin W, Geng X, Gu H, Zhan W, Zou Q, Yang Y. NeuroImage Automated brain tissue segmentation based on fractional signal mapping from inversion recovery Look – Locker acquisition. Neuroimage. 2010; 52(4):1347–54. [PubMed: 20452444]
20. Tassi L, Colombo N, Cossu M, Mai R, Francione S, Lo Russo G, et al. Electroclinical, MRI and neuropathological study of 10 patients with nodular heterotopia, with surgical outcomes. Brain. 2005; 128(2):321–37. [PubMed: 15618282]
21. Stefan H, Nimsky C, Scheler G, Rampp S, Hopfengärtner R, Hammen T, et al. Periventricular nodular heterotopia: A challenge for epilepsy surgery. Seizure. 2007; 16(1):81–6. [PubMed: 17134919]
22. Raza HK, Chen H, Chansysouphanthong T, Zhang Z, Hua F, Ye X, et al. The clinical and imaging features of gray matter heterotopia: a clinical analysis on 15 patients. Neurol Sci. 2019; 40(3):489–94. [PubMed: 30535564]
23. Liu W, Hu X, An D, Zhou D, Gong Q. Resting-state functional connectivity alterations in periventricular nodular heterotopia related epilepsy. Sci Rep. 2019; 9(1):1–9. [PubMed: 30626917]
24. Liu W, Yue Q, Tian Y, Gong Q, Zhou D, Wu X. Neural functional connectivity in patients with periventricular nodular heterotopia-mediated epilepsy. Epilepsy Res. 2021; 170:106548. [PubMed: 33454660]
25. Nune G, Arcot Desai S, Razavi B, Agostini MA, Bergey GK, Herekar AA, et al. Treatment of drug-resistant epilepsy in patients with periventricular nodular heterotopia using RNS® System: Efficacy and description of chronic electrophysiological recordings. Clin Neurophysiol. 2019; 130(8):1196–207. [PubMed: 31163364]
26. Franco AC, Peralta AR, Morgado C, Gonçalves Ferreira A, Rainha Campos A, Bentes C. Stereo-EEG recording and minimally invasive treatment of a periventricular nodular heterotopy: Two-in-one strategy. Clin Neurophysiol. 2020; 131(5):1099–101. [PubMed: 32200091]
27. Nolan RL, Brandmeir N, Tucker ES, Magruder JL, Lee MR, Chen G, et al. Functional and resting-state characterizations of a periventricular heterotopic nodule associated with epileptogenic activity. Neurosurg Focus. 2020; 48(2):E10.
28. Deleo F, Hong SJ, Fadaie F, Caldairou B, Krystal S, Bernasconi N, et al. Whole-brain multimodal MRI phenotyping of periventricular nodular heterotopia. Neurology. 2020; 95(17):e2418–26. [PubMed: 32817185]
29. Bloem JL, Reijnierse M, Huizinga TWJ, Van Der Helm-Van Mil AHM. MR signal intensity: Staying on the bright side in MR image interpretation. RMD Open. 2018; 4(1):e000728. [PubMed: 29955387]
30. Liao C, Wang K, Cao X, Li Y, Wu D, Ye H, et al. Detection of Lesions in Mesial Temporal Lobe Epilepsy by Using MR Fingerprinting. Radiology. 2018; 288(3):804–12. [PubMed: 29916782]
31. Hogan RE. Quantitative measurement of longitudinal relaxation time (qT1) mapping in TLE: A marker for intracortical microstructure? Epilepsy Curr. 2017; 17(6):358–60. [PubMed: 29217978]
32. Nöth U, Gracien RM, Maiworm M, Reif PS, Hattingen E, Knake S, et al. Detection of cortical malformations using enhanced synthetic contrast images derived from quantitative T1 maps. NMR Biomed. 2020; 33(2):1–15.
33. Hagiwara A, Fujimoto K, Kamagata K, Murata S, Irie R, Kaga H, et al. Age-Related Changes in Relaxation Times, Proton Density, Myelin, and Tissue Volumes in Adult Brain Analyzed by 2-Dimensional Quantitative Synthetic Magnetic Resonance Imaging. Invest Radiol. 2021; 56(3):163–72. [PubMed: 32858581]
34. Buonincontri G, Biagi L, Retico A, Cecchi P, Cosottini M, Gallagher FA, et al. Multi-site repeatability and reproducibility of MR fingerprinting of the healthy brain at 1.5 and 3.0 T. Neuroimage. 2019; 195:362–72. [PubMed: 30923028]
35. Körzdörfer G, Kirsch R, Liu K, Pfeuffer J, Hensel B, Jiang Y, et al. Reproducibility and Repeatability of MR Fingerprinting Relaxometry in the Human Brain. Radiology. 2019; 292(2):429–37. [PubMed: 31210615]
36. Hilbert T, Xia D, Block KT, Yu Z, Lattanzi R, Sodickson DK, et al. Magnetization transfer in magnetic resonance fingerprinting. Magn Reson Med. 2020; 84(1):128–41. [PubMed: 31762101]

37. Rugg-Gunn FJ, Boulby PA, Symms MR, Barker GJ, Duncan JS. Whole-brain T2 mapping demonstrates occult abnormalities in focal epilepsy. Neurology. 2005/01/26. 2005; 64(2):318–25. [PubMed: 15668431]

38. Salmenpera TM, Symms MR, Rugg-Gunn FJ, Boulby PA, Free SL, Barker GJ, et al. Evaluation of Quantitative Magnetic Resonance Imaging Contrasts in MRI-Negative Refractory Focal Epilepsy. Epilepsia. 2007; 48(2):229–37. [PubMed: 17295615]

39. Woermann FG, Barker GJ, Birnie KD, Meencke HJ, Duncan JS. Regional changes in hippocampal T2 relaxation and volume: a quantitative magnetic resonance imaging study of hippocampal sclerosis. J Neurol Neurosurg Psychiatry. 1998; 65:656–64. [PubMed: 9810933]

40. Bartolomei F, Khalil M, Wendling F, Sontheimer A, Régis J, Ranjeva J-P, et al. Entorhinal Cortex Involvement in Human Mesial Temporal Lobe Epilepsy: An Electrophysiologic and Volumetric Study. Epilepsia. 2005; 46(5):677–87. [PubMed: 15857433]

41. Cendes F, Andermann F, Gloor P, Evans A, Jones-Gotman M, Watson C, et al. MRI volumetric measurement of amygdala and hippocampus in temporal lobe epilepsy. Neurology. 1993/04/01. 1993; 43(4):719–25. [PubMed: 8469329]

42. Grinenko O, Li J, Mosher JC, Wang IZ, Bulacio JC, Gonzalez-Martinez J, et al. A fingerprint of the epileptogenic zone in human epilepsies. Brain. 2018; 141(1):117–31. [PubMed: 29253102]

43. Fisher RS, Webber WRS, Lesser RP, Arroyo S, Uematsu S. High-frequency EEG activity at the start of seizures. Vol. 9, Journal of Clinical Neurophysiology. 1992. p. 441–8. [PubMed: 1517412]

44. Wendling F, Bartolomei F, Bellanger JJ, Bourien J, Chauvel P. Epileptic fast intracerebral EEG activity: Evidence for spatial decorrelation at seizure onset. Brain. 2003; 126(6):1449–59. [PubMed: 12764064]

45. Thompson SA, Krishnan B, Gonzalez-Martinez J, Bulacio J, Jehi L, Mosher J, et al. Ictal infraslow activity in stereoelectroencephalography: Beyond the “DC shift.” Clin Neurophysiol. 2016; 127(1):117–28. [PubMed: 25920940]

46. Rodin E, Modur P. Ictal intracranial infraslow EEG activity. Clin Neurophysiol. 2008; 119(10):2188–200. [PubMed: 18782678]

47. Thompson SA, Krishnan B, Gonzalez-Martinez J, Bulacio J, Jehi L, Mosher J, et al. Interictal Infraslow Activity in Stereoelectroencephalography: From Focus to Network. J Clin Neurophysiol. 2016; 33(2):141–8. [PubMed: 26491857]

48. Jirsa VK, Stacey WC, Quilichini PP, Ivanov AI, Bernard C. On the nature of seizure dynamics. Brain. 2014; 137(8):2210–30. [PubMed: 24919973]

Key points

- High-resolution 3D MRF was used to characterize *in vivo* tissue property characteristics of PVNH.
- On individual level, MRF T_1 was significantly higher in SOZ than non-SOZ voxels; on group level, higher T_1 was also significantly associated with SOZ voxels.
- At the optimal cut-off of normalized T_1, a 76% accuracy for classifying SOZ nodules from non-SOZ nodules was achieved.
- MRF T_1 and T_2 values were significantly associated with SEEG ictal-onset power spectrum density at selected frequency bands.
- MRF can be used as a supplementary noninvasive tool to improve presurgical evaluation for patients with PVNH.

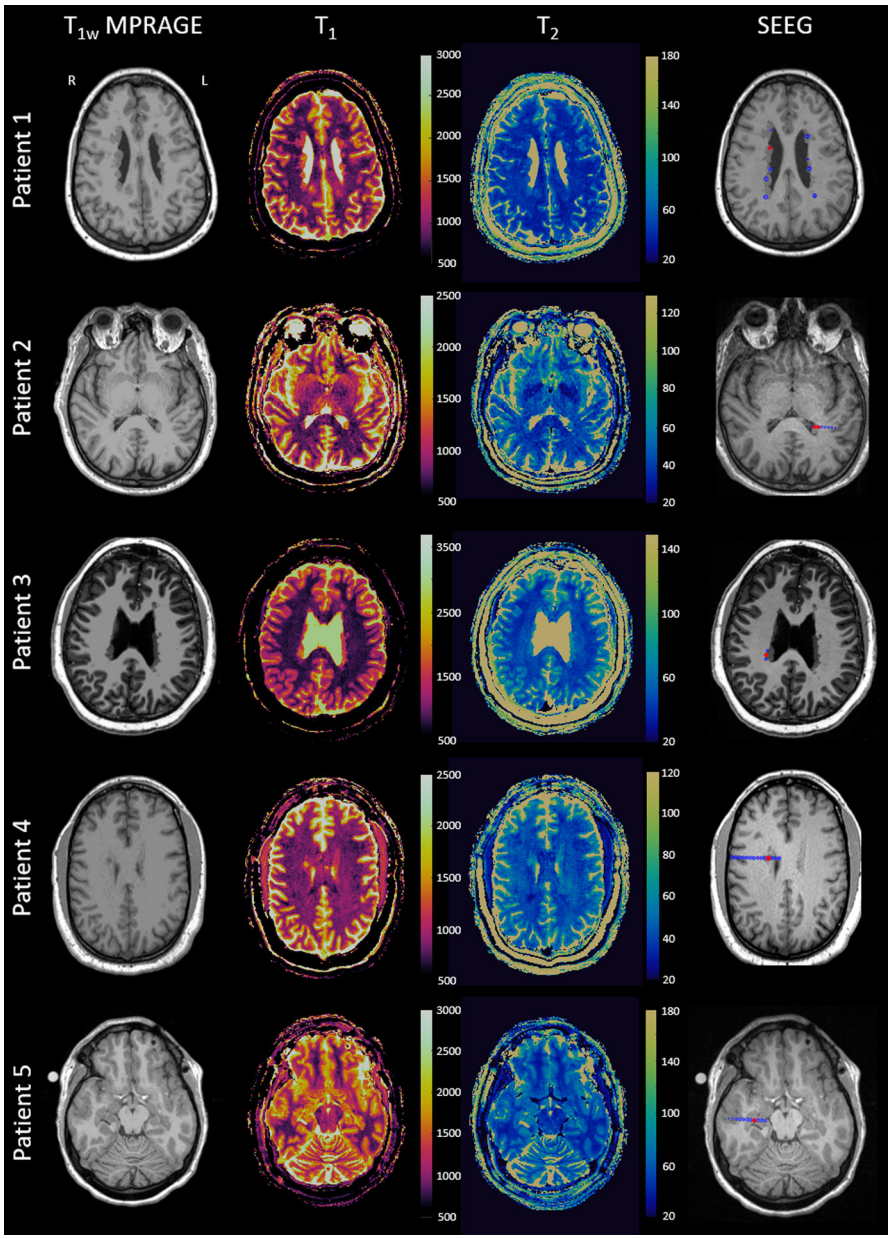

Figure 1. T1w MPRAGE image from clinical MRI, MRF T1 and T2 maps and SEEG implantations for the five epilepsy patients with PVNH included in this study.

The electrode contacts at the SOZ are marked with red and all implanted electrodes are marked with blue in the last column showing the implantations (only the contacts on the imaging plane are visualized). SEEG: stereotactic-electroencephalography.

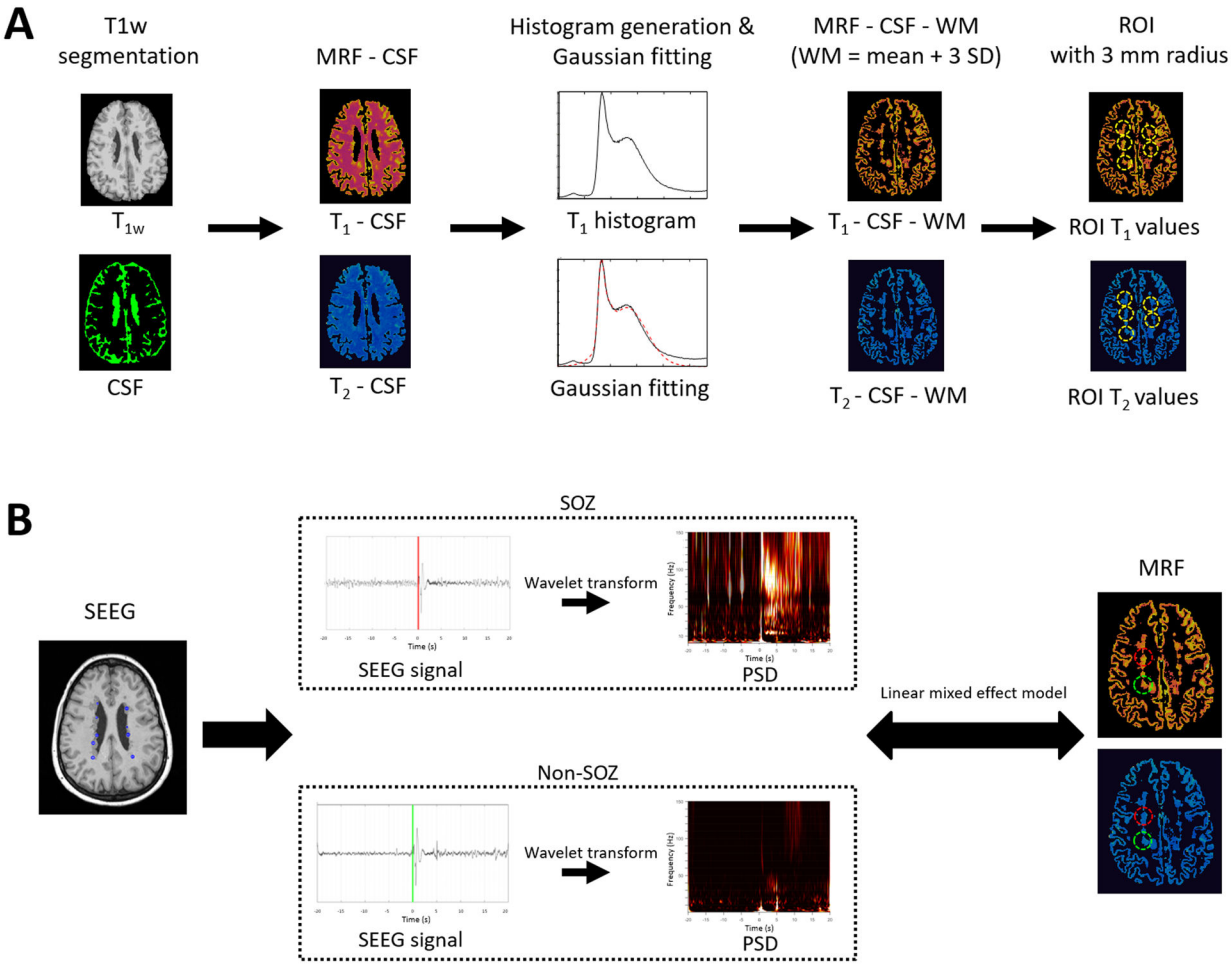

Figure 2. Diagram of study workflow.

(A) Extraction of T1 and T2 values from PVNH lesions. (B) Assessment of the correlations between T1 and T2 values and PSD of ictal-onset SEEG signals. Illustrated are the SEEG signals from SOZ nodule (red) and non-SOZ nodule (green). SEEG signals from both SOZ and non-SOZ nodules show high amplitude spike activity at the marked seizure onset. Compared to the non-SOZ nodule, the SEEG seizure pattern with the SOZ nodule consists of pre-ictal spiking followed by low-voltage fast activity at seizure onset. CSF: Cerebrospinal fluid. G-fitting: Gaussian fitting. WM: white matter. std: standard deviation. PVNH: periventricular nodular heterotopia. PSD: power spectral density. SEEG: stereotactic-electroencephalography. ROI: region of interest. SOZ: seizure onset zone. The mean and standard deviation of WM are calculated by the Gaussian fitting of the histogram. PSD is calculated by applying wavelet transform of SEEG signals at the seizure onset zone window. Red color denotes SOZ and green color denotes non-SOZ nodules for illustrative purpose. Markings on SEEG signal indicates the ictal onset obtained from clinical charts.

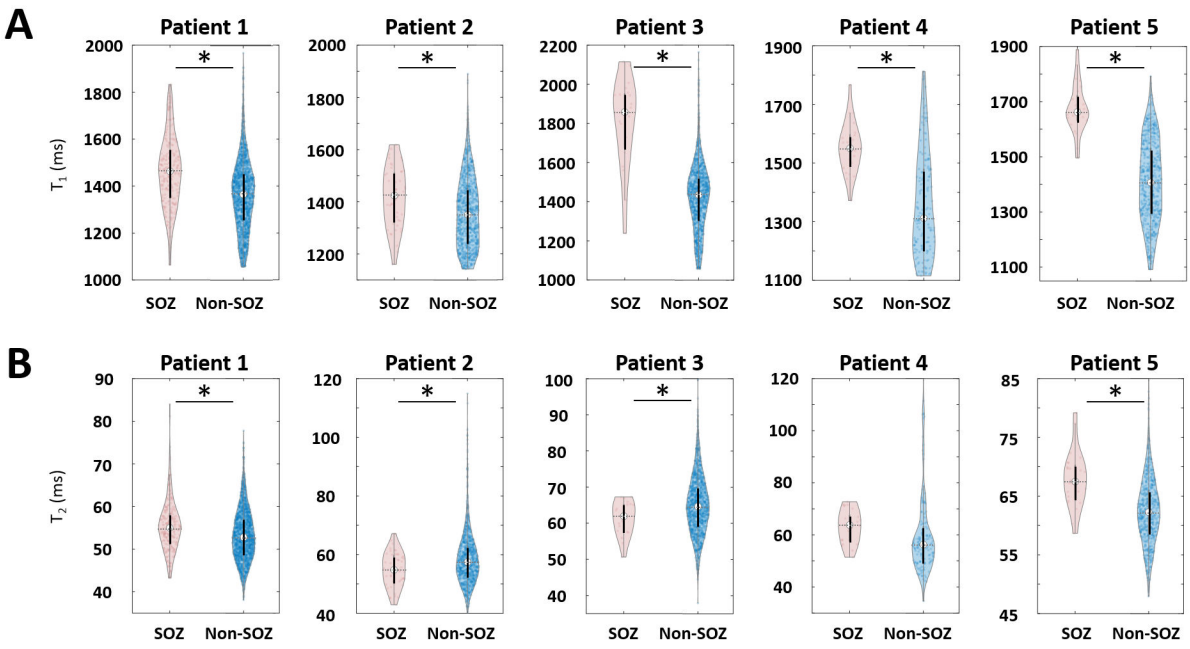

Figure 3. Violin plots of MRF T1 (A) and T2 (B) values showing all the SOZ and non-SOZ voxels.

On each plot, the center indicates the median value of all voxels. SOZ: seizure onset zone.

Table 1.

Clinical and demographic data of the study cohort.

Pt	Sex	Age (yr)	Hand	Onset age (yr)	Epilepsy duration (yr)	Seizure frequency	PVNH MRI Impression[a]	Cortical malfomation[a]	# of total (nodule) SEEG electrodes[b]	SEEG-detected SOZ	Surgery	Pathology[c]	Seizure outcome[d]
1	F	42	R	31	9	10–15/m	Bilateral, Multiple	None	15 (13)	PVNH	Bilateral nodule ablation	NA	ILAE-2
2	M	56	R	5	51	Daily	Bilateral, Multiple	None	14 (5)	PVNH	Uni lateral nodule ablation	NA	ILAE-1
3	F	20	R	16	4	1–7/m	Bilateral, Multiple	None	13 (5)	PVNH + cortex	Uni lateral nodule + cortex ablation	NA	ILAE-1
4	M	45	R	37	8	1/w	Unilateral, Multiple	None	16 (1)	PVNH + cortex	Uni lateral nodule + cortex ablation	NA	ILAE-3[e]
5	F	16	R	8	8	1–2/m	Bilateral, Multiple	None	19 (6)	PVNH+ cortex	Uni lateral nodule + cortex resection	Heterotopia, no FCD, No HS	ILAE-1

[a] MRI impression was based on the official radiology report.

[b] Number of total SEEG electrodes used, with the number of electrodes targeting nodules in parentheses.

[c] Pathology was classified based on the ILAE 2016 recommendation of the neuropathologic workup of epilepsy surgery brain tissue and the ILAE 2011 FCD classification guidelines.

[d] Surgical outcome was defined by the ILAE classifications.

[e] This patient only had two seizures after surgery (as compared to weekly seizures before).

Pt: patient. yr: year. PVNH: periventricular nodular heterotopia. SEEG: Stereotactic-electroencephalography. SOZ: seizure onset zone. F: female. M: male. R: right. L: left. m: month. w: week. NA: not available (due to laser ablation). FCD: focal cortical dysplasia. HS: hippocampal sclerosis.

Table 2.

Mean and standard deviation of MRF T_1 and T_2 values in voxels from SOZ and non-SOZ nodules.

	T_1 (ms)		T_2 (ms)		P value[a]	P value[b]
	SOZ	Non-SOZ	SOZ	Non-SOZ		
Patient 1	1461 ± 153	1362 ± 149	55.4 ± 6.0	53.3 ± 6.0	< 0.001	< 0.001
Patient 2	1418 ± 112	1358 ± 133	54.8 ± 5.8	58.7 ± 9.2	0.0025	0.0044
Patient 3	1804 ± 227	1422 ± 174	61.4 ± 4.7	65.1 ± 8.1	< 0.001	0.0423
Patient 4	1553 ± 85	1359 ± 180	63.3 ± 6.3	61.0 ± 19.3	< 0.001	0.5620
Patient 5	1675 ± 89	1410 ± 148	67.8 ± 4.7	62.4 ± 5.7	< 0.001	< 0.001

[a] P value is obtained from T_1 of SOZ and that of non-SOZ.

[b] P value is derived from T_2 of SOZ and that of non-SOZ.

SOZ: seizure onset zone. P values are derived from a T-test between SOZ and non-SOZ voxels ($p^* < 0.05$).

Table 3.

Classification performances (based on the Youden index) to differentiate voxels from SOZ and non-SOZ nodules at the individual patient-level.

	T_1					T_2				
	ACC (%)	**SEN (%)**	**SPE (%)**	**AUC**	**Cutoff (ms)**	**ACC (%)**	**SEN (%)**	**SPE (%)**	**AUC**	**Cutoff (ms)**
Pt 1	66.8	58.8	67.8	0.68	1429	55.1	65.4	53.8	0.6025	53.3
Pt 2	59.9	64.6	59.6	0.64	1386	58.9	59.1	56.3	0.6179	55.6
Pt 3	82.1	90.0	82.0	0.90	1561	47.5	46.9	80.0	0.6397	65.3
Pt 4	73.6	92.0	70.6	0.82	1455	71.9	64.0	73.2	0.6897	61.6
Pt 5	84.5	91.7	84.2	0.95	1584	74.2	70.8	74.3	0.7783	65.7
Average	73.4	79.4	72.8	0.80	1483	61.5	61.2	67.5	0.6656	60.3

Pt: patient. SOZ: seizure onset zone. ACC: accuracy. SEN: sensitivity. SPE: specificity. AUC: area under the receiver operating characteristic curve.